Published in final edited form as:
Biomaterials. 2012 May ; 33(15): 3824–3834. doi:10.1016/j.biomaterials.2012.01.048.

Microfabrication of complex porous tissue engineering scaffolds using 3D projection stereolithography

Robert Gauvin[a,b,c,1], **Ying-Chieh Chen**[a,b,c,1], **Jin Woo Lee**[d,1], **Pranav Soman**[d], **Pinar Zorlutuna**[a,b], **Jason W. Nichol**[a,b], **Hojae Bae**[a,b], **Shaochen Chen**[d,**], and **Ali Khademhosseini**[a,b,c,*]

[a]Center for Biomedical Engineering, Department of Medicine, Brigham and Women's Hospital, Harvard Medical School, Cambridge, MA, USA

[b]Harvard-MIT Division of Health Sciences and Technology, Massachusetts Institute of Technology, Cambridge, MA, USA

[c]Wyss Institute for Biologically Inspired Engineering, Harvard Medical School, Boston, MA, USA

[d]Department of NanoEngineering, University of California, San Diego, Atkinson Hall, MC-0448, 9500 Gilman Drive, La Jolla, CA 92093-0448, USA

Abstract

The success of tissue engineering will rely on the ability to generate complex, cell seeded three-dimensional (3D) structures. Therefore, methods that can be used to precisely engineer the architecture and topography of scaffolding materials will represent a critical aspect of functional tissue engineering. Previous approaches for 3D scaffold fabrication based on top-down and process driven methods are often not adequate to produce complex structures due to the lack of control on scaffold architecture, porosity, and cellular interactions. The proposed projection stereolithography (PSL) platform can be used to design intricate 3D tissue scaffolds that can be engineered to mimic the microarchitecture of tissues, based on computer aided design (CAD). The PSL system was developed, programmed and optimized to fabricate 3D scaffolds using gelatin methacrylate (GelMA). Variation of the structure and prepolymer concentration enabled tailoring the mechanical properties of the scaffolds. A dynamic cell seeding method was utilized to improve the coverage of the scaffold throughout its thickness. The results demonstrated that the interconnectivity of pores allowed for uniform human umbilical vein endothelial cells (HUVECs) distribution and proliferation in the scaffolds, leading to high cell density and confluency at the end of the culture period. Moreover, immunohistochemistry results showed that cells seeded on the scaffold maintained their endothelial phenotype, demonstrating the biological functionality of the microfabricated GelMA scaffolds.

Keywords

Microfabrication; Three dimensional printing; Scaffold; Mechanical properties; Confocal microscopy; Cell proliferation

[*]Corresponding author. Department of Medicine, Brigham and Women's Hospital, Harvard Medical School, PRB, Rm 252, 65 Landsdowne Street, Cambridge, MA 02139, USA. Tel.: +1 617 388 9271; fax: +1 617 768 8202. [**] Corresponding author. Tel.: +1 858 822 7856; fax: +1 858 534 9553. Chen168@ucsd.edu (S. Chen), alik@rics.bwh.harvard.edu (A. Khademhosseini).
[1]These authors contributed equally to this work.

Appendix. Supplementary material

Supplementary material associated with this article can be found, in the online version, at doi:10.1016/j.biomaterials.2012.01.048.

1. Introduction

The aim of tissue engineering is to develop biological substitutes that will restore lost morphological and functional features of diseased or damaged organs [1]. Human tissues are mostly comprised of cells and extracellular matrix (ECM) elements, which regulate the biological, physical and chemical cues of the microenvironment and play a critical role in modulating cell function and behavior. Scaffolding materials intended for tissue engineering applications are designed to closely mimic the physiologic environment, including the geometrical, topographical and physical features of the targeted tissue [2,3]. The ability to fabricate three dimensional (3D) scaffolds having specifically designed microarchitecture reproducing the *in vivo* environment could elicit a physiologically relevant response and result into improved functionality of the tissue [4].

The field of tissue engineering has so far provided technologies that are adequate for the replacement of connective tissues such as skin [5], cartilage [6], bladder [7] and blood vessels [8]. However, it is becoming clear that more complex tissues, having specific microarchitecture or extensive vascular networks, may require more precise structures. To produce microctructured scaffolds, multiple techniques such as solvent casting [9], particulate leaching [10,11], gas foaming [12], freeze drying [13] and more recently electrospinning [14] and laser sintering [15] have been developed. Many of these scaffolds have been shown to produce structures allowing for cell adhesion and migration throughout the biomaterial. However, these methods are limited since pore size and interconnectivity are often process driven as opposed to rationally designed, which reduces the role of the scaffold microenvironment in directing cell behavior. Microscale features such as anisotropy, known to guide bone regeneration along the principal directions of porosity [16] and stiffness gradient, which can regulate stem cell differentiation [17], can be used to enhance tissue function. Precisely defined accordion-like microstructures having biomimetic mechanical properties were shown to mimic the function of adult rat right ventricular myocardium [18] and microengineered 3D porous structure of a multi-layered elastomeric scaffolds allowed heart cells to be readily seeded by perfusion throughout the full thickness of a tissue engineered myocardium [19]. Micron scale struts geometry in 3D collagen-glycosaminoglycan scaffolds have also been shown to correlate with increased fibroblast migration speed and induced changes in cell persistence [20]. Thus, scaffold design, architecture and properties are of the utmost importance for adequate functionality *in vitro* and *in vivo*.

Hydrogel biomaterials have been of particular interest for numerous years in tissue engineering and 3D cell culture due to their close resemblance to native connective tissues. However, they have limited capabilities when it comes to generating complex tissue structures dependent on precise cell and ECM organization. Platforms allowing for the regeneration of organs such as the liver and the kidney, requiring functional units and vasculature, have yet to be developed. Recent advances in hydrogel chemistry and cell biology have resulted into scaffolding materials aiming to mimic spatial organization of cells and ECM molecules found in vivo. Moreover, photopolymerizable networks have enabled encapsulation of cells and bioactive molecules in hydrogels and new technologies controlling the arrangement of cells and molecules at the microscale have been developed [21–24]. Microfabrication techniques such as soft lithography, photolithography, microfluidics and 3D printing have emerged from automotive, microelectronics and aerospace industries and have recently been translated to applications in biological sciences. These technologies have successfully been integrated into the field of tissue engineering and have enhanced tissue functionality through control of the microenvironment [25,26]. Adhesion motifs, growth factors and proteolytic sequences have all been incorporated to hydrogels to guide cellular processes such as migration, proliferation and differentiation, as

well as to trigger degradation kinetics of scaffolding materials [27–29]. Traditional design limitations, often related to mold shape and processing, were overcome by the use of these microfabrication methods, allowing for the generation of intricate structures [22,30]. However, most patterning techniques intended to create tissues and to study cell behavior have been developed for two dimensional (2D) applications and the use of standard photomasks for the fabrication of 3D hydrogels comprising of complex structures requires a high level of precision and is time consuming.

Advances in photolithographic techniques have broadened the capability to produce 3D hydrogel structures in a rapid and reproducible fashion [31]. Important parameters of scaffold design are the ability to control the architecture and the mechanical behavior of the material to provide the cells with access to nutrients into a stable 3D structure. Manufacturing and fabrication technologies such as rapid prototyping [32,33], laser microstereolithography [34–36] and solid freeform fabrication (SFF) have evolved as methods to fabricate 3D scaffolds with micrometer scale resolution by using Computer-Aided-Design (CAD) programs [37]. However, the time required for these fabrication processes is currently a major limitation. For example, scaffold fabrication using laser-microstereolithography (SL) requiresa long process due to the point-by-point laser scanning procedure [38] and post-fabrication procedures [39]. As opposed to the 2D raster scanning style of SL, a digital micro-mirror device projection printing (DMD-PP) system has the capability to fabricate an entire layer under one single UV exposure, thereby leading to high manufacturing speed [31,40–42]. A 3D scaffold can be fabricated using this method by projecting a dynamic pattern on a photocurable monomer, resulting in a layer-by-layer fabrication approach. The solid structure in each layer is formed by photopolymerization, the light pattern being controlled by the micro-mirrors in the DMD apparatus. The physical characteristics of the scaffold such as porosity and interconnectivity can be tailored using this system, by precisely controlling pore geometry and architecture, therefore influencing diffusion, fluid flow, mechanical properties as well as cell behavior.

In the present study, a custom designed projection stereolithography (PSL) system was used to control the 3D microarchitecture of collagen-based gelatin methacrylate (GelMA) hydrogels [21,43]. The addition of methacrylamide moieties to the side groups of natural gelatin enables photopolymerization of the hydrogel, thus intricate structures supporting cell adhesion and growth can be engineered. Specifically, 3D layer-by-layer photolithography was used to generate hydrogels having either wood pile or hexagonal porous structures for different prepolymer concentrations. Other investigators have previously designed highly porous and biophilic structures relying on Triply Periodic Minimal Surfaces (TPMS) models [36,44,45]. TPMS designed scaffolds have been produced by computer-aided stereolithography. Gyroid and diamond shaped pores [39], as well as periodic surfaces created using simple trigonometric functions [45] have been shown to enable the generation of scaffolds that can be used for various tissue engineering applications. More recently, sophisticated structures have been designed by combining TPMS, distance field and optimized hexahedral elements to produce porous scaffolds having intricate internal architecture and high quality external surface [46]. In the current study, it is demonstrated that simple scaffold design parameters, such as struts geometry and assembly, as well as polymer concentration, can be used to enable control over the mechanical properties of the material. Endothelial cells were seeded on the scaffold to demonstrate the capability of the 3D engineered structures to support cell adhesion and proliferation. The combination of the PSL apparatus with GelMA, a photocrosslinkable collagen-based hydrogel, resulted into 3D scaffolds on which endothelial cells attached and proliferated. Besides enabling cells to be cultured into a 3D structure having defined spatial architecture, this work highlights the fact that scaffold fabrication could benefit from the introduction of a computerized and automated high-throughput process.

2. Materials and methods

2.1 Gelatin methacrylate synthesis

GelMA was synthesized as described previously [21]. Briefly, porcine skin gelatin (Sigma Aldrich, St. Louis, MO, USA) was mixed at 10%(w/v) into phosphate buffered saline (PBS; Gibco, Billings, MT, USA) and stirred at 60 °C until fully dissolved. Methacrylic anhydride (MA; Sigma) was added to the solution at a rate of 0.5 ml/min until a concentration of 8% (v/v) of MA was obtained in the gelatin solution. The solution was then stirred for 1 h at 50 °C, followed by a 2x dilution with warm PBS and dialyzed against distilled water using 12–14 kDa cutoff dialysis tubing (Spectrum Laboratories, Rancho Dominguez, CA, USA) for one week at 40 °C to remove the unreacted groups from the solution. The GelMA solution was frozen overnight at −80 °C and lyophilized in a freeze dryer (Labonco, Kansas City, MO, USA) for one week. Freeze dried GelMA foam was stored at −80 °C until further usage.

2.2. Hydrogel prepolymer preparation

Freeze dried GelMA macromer was mixed into PBS at a 10% or 15% concentration and stirred at 60 °C until fully dissolved. Calcium chloride and sodium carbonate (20%(w/v) Fisher Scientific, Fair Lawn, NJ, USA) was added to the GelMA solution and stirred for 24 h until precipitation of sodium chloride, resulting into a solution of GelMA and calcium carbonate microparticles. Photoinitiator (1%(w/v), Irgacure 2959, CIBA Specialty Chemicals, Basel, Switzerland), UV absorber (0.1% (w/v) HMBS, (2-hydroxy-4-methoxy-benzphenone-5-sulfonic acid), Sigma) and solution quencher (0.01% (w/v), TEMPO, Sigma) were added to the solution to allow for photo-polymerization and provide efficient cure depth and optimal pattern resolution.

2.3. Scaffold fabrication method

A PSL apparatus was used to produce the 3D scaffolds through UV photolithography in a layer-by-layer fashion (Fig. 1A) [40]. Briefly, a digital light processing (DLP) chip (Discovery 4000, Texas Instrument, TX, USA) was used to create active and reflective dynamic photomasks from a CAD drawing (AutoCad, Autodesk, San Rafael, CA, USA). These dynamic photomasks were used to reproduce cross-sectional images of the 3D microstructure (Fig. 1B – G) and project the patterns onto the prepolymer solution using a uniform UV light source (EXFO, Quebec, QC, Canada). These patterns were irradiated for 20 s at an intensity of 50 mW/cm^2 through a UV-grade optical lens (Edmunds Optics, Barrington, NJ, USA) onto the fabrication stage located at the focal point of the projection lens. This process created a layer-by-layer 3D microstructure by UV polymerization of the prepolymer solution. A glass coverslip was placed above the microstructure to control the thickness of each microstructure layer. Consequently, 3D structures were created by sequential development of the hydrogel accordingly to the cross-sectional images generated on the PSL chip (Fig. 2). Following the fabrication procedure, scaffolds were removed from the stage and gently washed using PBS. Calcium carbonate residues were removed by rinsing the scaffolds in HCl (0.01 M, Sigma) solution for 24 h prior to cell seeding [47,48] (Fig. 1H).

2.4. FTIR spectrum

Characterization of the chemical structure of the material was performed by Fourier transformed infrared spectroscopy (FTIR; Nicolet 6700, ThermoScientific, Rockford, IL, USA). FTIR spectra were acquired with Smart-iTR using a N_2 purged sample chamber. The acquisition parameters were set to 128 scans with a 4 cm^{-1} spectra resolution (Fig. 1H).

2.5. Mechanical testing

Unconfined compression testing was performed on the microfabricated 3D rectangular scaffolds (5×5 mm; $h = 1$ mm) (Fig. 3). Hydrated samples were placed between two compression plates and were loaded at a strain rate of 20% per minute using a mechanical tester (Instron, Norwood, MA, USA). Low strain and high strain moduli were defined as the slope of the linear portion of the stress-strain curve comprised between 20–40% and 70–90% strain respectively (Fig. 3A). Stress-strain curves were plotted and analyzed using an in house developed Matlab® script (The Mathworks, Natick, MA, USA) to facilitate the calculation of the testing parameters. Error bars represent standard deviation with $n = 5$ (Fig. 3B). Statistical significance was determined with ANOVA followed by a post-hoc Tukey test, using a standard $p < 0.05$ (Minitab, State College, PA. USA).

2.6. Cell culture

Immortalized human umbilical vein endothelial cells constitutively expressing green fluorescent protein (HUVEC-GFP, generous donation from the laboratory of the late Dr. J.Folkman, Children's Hospital, Boston, MA, USA) were cultured in endothelial basal medium (EBM-2; Lonza, Allendale, NJ, USA) supplemented with 20% foetal bovine serum (FBS; Hyclone, Logan, UT, USA) endothelial growth bulletkit (Lonza) and antibiotics (1% penicillin/streptomycin (P/S), Sigma) in 75 cm^2 tissue culture flasks (BD Biosciences, Bedford, MA, USA). Cells were passaged 2 times per week and media was changed every 2 days. Cells were kept in a standard cell culture incubator, 5% CO_2 and 37 °C.

2.7. Cell seeding of the scaffolds

The PSL-fabricated scaffolds were incubated overnight in a solution of antibiotics and were rinsed using PBS. HUVEC-GFP were trypsinized, counted and resuspended in fresh media at a density of 20,000 cells/ml in a 1.5 ml tube (Eppendorf, Hauppauge, NY, USA). Scaffolds were put in the cell suspension and incubated under constant agitation (4 rpm) in a 3D orbital rotating shaker (Glas-Col, Terre Haute, IN, USA) for 12 h to provide a dynamic cell seeding environment. The cell-seeded scaffolds were then transferred into a 12-wells plates and cultured as previously described (Fig. 4).

2.8. Cell viability

Cell survival and proliferation was measured on days 1, 4 and 7 after seeding (Fig. 4E). CellTiter 96® AQ_{ueous} One solution reagent (Promega, Madison, WI, USA) was used for quantification. Briefly, cell-seeded constructs were washed with cell culture media without phenol red (DMEM, Gibco) and incubated in the presence of the reagent in a 1:5 dilution in DMEM. The absorbance was measured at 490 nm following 2 h of incubation at 37 °C and 5% CO_2. All measurements were normalized to day 1 and results are presented as mean +/− standard deviation ($n = 3$).

2.9. Cell adhesion and coverage of the scaffolds

Scaffolds were mounted on glass-bottom dishes (MatTek, Ashland, MA, USA) and imaged using an inverted laser scanning confocal microscope (Leica SP5XMP, Buffalo Grove, IL, USA). Multiple consecutive optical sections were acquired starting at the bottom surface of the specimen. These images were later stacked and rendered in three dimensions using the BitplaneImaris 7.1 software (Bitplane, South Windsor, CT, USA). Cell morphology and spreading were visualized by imaging of the green fluorescence of HUVECs-GFP (Figs 5,6). Total cell coverage was quantified on 3D reconstruction confocal images using the Image J software (NIH, Bethesda, Maryland) (Fig. 6G).

2.10. Immunohistochemistry

The cell-seeded scaffolds were incubated with anti-human CD31 (DakoCytomation, Carpintera, CA, USA), vonWillebrand Factor (vWF; DakoCytomation), phalloidin-Alex488 (Invitrogen, Carlsbad, CA, USA) and anti-Ki67 (Millipore, Bill-erica, MA, USA) antibodies for immunofluorescence labeling. Briefly, the scaffolds were fixed in 4% paraformaldehyde, permeabilized with 0.5% Tween (BioRad, Hercules, CA, USA) in PBS for 10 min and maintained in a bovine serum albumin solution (BSA, 1.5%; Sigma) for 30 min. The scaffolds were then incubated overnight at 37 °C in presence of the primary antibodies (1:100 dilution), washed three times in PBS and incubated with Alexa Fluor 488-conjugated goat anti-mouse and anti-rabbit secondary antibodies (Invitrogen; 1:200 dilution) for 1 h at room temperature. Finally, scaffolds were stained with DAPI, immersed in PBS, and examined using a confocal microscope (Leica). 3D images reconstructions were performed using the BitplaneImaris software (Fig. 7).

3. Results

3.1. Scaffold fabrication

A custom made PSL apparatus [40] was used to microfabricate GelMA hydrogel scaffolds having precise porous structures (Figs. 1 and 2). This setup allowed for the layer-by-layer engineering of scaffolds having dimensions that were less than 200 μm. GelMA was previously shown to be non-cytotoxic and compatible with micropatterning techniques [21,49]. This material was used to prepare a liquid prepolymer solution and processed through the 3D photolithographic automated PSL process. GelMA prepolymer was reinforced with non-cytotoxic $CaCO_3$ microparticles during the fabrication. The composite scaffolds were incubated in a HCl solution to dissolve the embedded $CaCO_3$ microparticles within the scaffolds, and rinsed thoroughly with PBS prior to cell seeding. The presence of remaining $CaCO_3$ in the material following the PSL fabrication process was verified by the peaks of CO_3^{2-} (1410–1450 cm^{-1}, 870 cm^{-1}) on the collected spectrum, showing complete removal of the residues following incubation in the HCl solution (Fig. 1H). Scaffolds of different internal pore architectures were produced using woodpile and hexagonal shapes previously designed using a CAD software (Fig. 1B–G, Fig. 2). The custom designed setup, comprised of a x-y-z motorized platform immersed in the liquid prepolymer, was selectively exposed to a focused UV laser light. Irradiated sections of the polymer became solid whereas non-irradiated areas remained liquid. This liquid was rinsed following the crosslinking procedure, leaving only an open porous structure. As shown in Fig. 2, this process resulted into scaffolds having rectangular or hexagonal pores. PSL processing parameters were chosen in order to obtain similar porosity and feature size for all scaffold types. This was done to assess solely the effect of pore network architecture on mechanical properties (Fig. 3) and to provide the cells a relatively high surface area to attach on the scaffold (Fig. 4). To explore the capability of the technique, both single and multilayered constructs were fabricated (Fig. 5). Multi-layered constructs were analyzed for cell coverage using confocal microscopy (Fig. 6), whereas single layer construct were used to analyze the biological functionality of the scaffolds (Fig. 7).

3.2. Mechanical properties

The mechanical properties of the scaffolds were measured in order to investigate the influence of pore architecture on the compressive modulus of the microfabricated structures (Fig. 3). The response of the porous scaffolds was found to be similar for every structure tested. A biphasic stress-strain relationship comprised of a low strain (20–40%) and a high strain (70–90%) behavior was observed for both woodpile and hexagonal structures (Fig. 3A). The low-strain response could be explained by the realignment and the reorganization

of the struts during the first phase of compression. The low-stain modulus was found to be similar for every condition tested, regardless of feature shape and prepolymer concentration (Fig. 3B). The high-strain response was initiated at a strain level where struts reorganization becomes impossible due to the close packing of the porous structure. Significant differences were observed at high-stain levels, where both prepolymer concentration and scaffold design were found to influence the modulus of the scaffolds (Fig. 3C, D). Interestingly, no scaffold experienced catastrophic failure during compression, every sample recovering its original shape a short time after being submitted to the test (not shown). The compressive properties measured at lower and higher strain were respectively relative to the amount of reorganization allowed by the structure and by the properties of the material being compressed. Taken together, these results demonstrate the capability of the PSL fabrication method to tailor the mechanical properties of the scaffolds by varying the prepolymer concentration and the CAD drawing used for scaffold design and fabrication.

3.3. Cell-seeded scaffolds

HUVEC cells expressing GFP were seeded on the microfabricated GelMA scaffolds to evaluate the capability of the constructs to enable cell adhesion, spreading and proliferation (Fig. 4). Cell spreading was easily visible under fluorescent microscopy due to the GFP constitutively expressed by the HUVECs. Cell spreading involves the activation of actin polymerization and myosin contraction, which indicate cell viability and function [34]. These GelMA scaffolds show a potential advantage as previous studies have demonstrated and since cells do not spread on a number of synthetic hydrogels without the inclusion of adhesive peptides sequences [50–52]. Moreover, cells seeded on the hydrogel structures remained viable for extended incubation period showing the adequate biocompatibility of the scaffold. The number of cells present on the scaffold, measured by the MTS assay, increased as a function of time until the formation of a confluent laver of HUVECs on the surface (Fig. 4E).

The initial cell adhesion and scaffold coverage was favored by using a dynamic seeding approach, allowing the cells to penetrate into the porous structure during the process (Fig. 5). The surface coverage of the scaffold during the culture period was quantified by analyzing images from 3D confocal microscopy (Fig. 6). Results showed a constant increase in cell density on the surface from day 1 until day 4, where the entire thickness of the scaffold was covered by a confluent layer of cells (Fig. 6A–C, G). Higher magnification of the cell seeded scaffolds was used to visualize cell penetration in the 3D porous structure. Similar results were found as the cell density through the thickness of the material increased as a function of the culture period (Fig. 6D – F). These results suggest that the cells seeded on the scaffolds spread and proliferated until a confluent layer of HUVEC was obtained and covered the surface of the material. This also demonstrates that open architecture of the scaffold facilitates the infiltration of a cell suspension into the 3D structure of the scaffold.

Immunostaining assays were performed on the cell seeded scaffolds in order to investigate if the seeding and culture processes influenced cell behavior and phenotype. HUVEC were found to express endothelial cells markers such as CD31 (Fig. 7A) and vWF (Fig. 7B), suggesting their ability to retain their normal phenotype following seeding, adhesion and proliferation on the GelMA scaffolds. Moreover, Ki67 labeling of the nucleus showed that a certain percentage of cells were still in a proliferative state after 4 days in culture (Fig. 7C – D). Taken together, these results indicate that the microfabricated, porous GelMA scaffolds can support cell adhesion and proliferation for an extended period of time, without jeopardizing the biological function and phenotype of the cells.

4. Discussion

A versatile layer-by-layer microfabrication system was used in combination with photocrosslinkable GelMA hydrogels to produce scaffolds integrating cells in a complex 3D microarchitecture. This PSL apparatus was previously fabricated and used to create 3D PEG-based biological scaffolds with complex internal architectures and spatial patterns in a high throughput fashion [31,40]. The use of this system in combination with PEG hydrogels has proven useful for the study of osteogenic differentiation of murine bone marrow stromal cells as well as Schwan and glial cells behavior on EDC-NHS modified PEG [41]. In a recently published paper, a PSL apparatus was also used to impart negative Poisson's ratio property to PEG hydrogel using cellular structures (pores) having special geometries, arrangements, and deformation mechanisms [53]. The current study describes the fabrication of 3D scaffolds from a photopolymerizable gelatin-based prepolymer solution through UV photolithography, using a dynamic pattern generator in which the microstructures are developed in a layer-by-layer approach. These scaffolds were shown to possess intricate internal geometries allowing for cell adhesion, migration and proliferation.

One of the essential criteria to develop functional engineered tissues is to reproduce the 3D tissue architecture and provide a biologically relevant environment to the cells in order for them to maintain viability and to proliferate on the scaffolding material [20,54,55]. Interconnections between pores also play an important role in cell seeding, migration and nutrient transport during culture of the scaffolds [39,56]. Cell seeded porous scaffolds often display hypoxia induced cell death in their bulk due to the lack of nutrients diffusing within the 3D environment [57,58]. Therefore, the use of porous structures having uncontrolled architectures compromise the quality of engineered grafts and the success of *in vivo* applications. Many groups have recently developed photopatterning approaches to fabricate scaffolds displaying 3D microfabricated structures [22,30,31,34] and biophilic geometries TPMS designs [39,44,45]. These studies clearly demonstrate the benefit of controlling the cellular microenvironment to reproduce the architecture of biological tissues [59]. However, most of this work has involved synthetic polymers such as PEG, which requires the grafting of adhesive peptides such as RGD or coating with proteins to enhance cell interaction with the scaffold [60–62]. The advantage of using naturally derived hydrogels such as GelMA, is the presence of biologically active sequences that bind key integrins that enable cells to adhere and migrate onto the 3D structure. It also provides built-in degradable moieties, which usually need to be added to synthetic polymers [28]. It can also be used to encapsulate cells, is compatible with microfabrication processes and allow tissue growth for extended periods of time [21,49].

The utility of the current method was demonstrated by producing hexagonal and log pile GelMA structures. Scaffold properties at the microscale are known to influence cell-ECM interactions and to dictate the mechanical properties and degradation behavior of a biomaterial [25]. Since many scaffolds are required to fill space and provide a framework for the tissue they intend to replace, it is important to be aware of the mechanical properties of biomaterials. Moreover, it is essential to have enough surface area for the cells to attach and big enough pores to allow for nutrient transport, vascularization and tissue ingrowth in the material. Therefore, a balance between structure, function and strength needs to be engineered. The mechanical properties rely on factors such as the network crosslinking density and polymer concentration. However, it is difficult to predict the physical properties of a microfabricated hydrogel network based only on the knowledge of macromer structure. Other parameters such as crosslinking mechanism and polymer concentration also play a role in these properties [21]. The design of precise and specific structures in the material also has the capability to tailor the mechanical properties of a 3D hydrogel material [63,64]. The measurement of the compressive properties of the microfabricated 3D GelMA

hydrogels resulted in biphasic stress-strain curves, which can be explained by the level of deformation applied prior and following the maximum degree of reorganization of the porous structures. Following the low-strain phase, the stress-strain relationship behaved linearly as if a solid element was tested and compression results measured were similar as the sole properties of an elastic material. Results obtained were found to be within a physiologic range (0–800 kPa) [65] and prepolymer concentration and scaffold geometry were shown to enable the tailoring of the mechanical properties of the hydrogels. The microfabricated GelMA scaffolds also supported cell adhesion, migration and proliferation, demonstrating the potential of this approach for the fabrication of 3D constructs for tissue engineering applications. Moreover, the HUVEC seeded on the scaffold formed a confluent monolayer and retained their endothelial phenotype, as indicated by the presence of CD31 and vWF markers 4 days following the dynamic seeding process (Fig. 7).

The PSL microfabrication setup allowed for high-speed generation of microengineered 3D structures. Results obtained in combination with GelMA demonstrated the ability of the system to generate scaffolds favoring cell adhesion and proliferation in a spatially regulated fashion. This technique could become useful for customized tissue engineering strategies, since only a CAD file is required to produce the geometry of the scaffold and that features as small as 10 microns can be generated. Therefore, it would be possible to precisely engineer a tissue scaffold using a converted image file from a MRI or a CT-scan taken directly on the patient. We are currently moving towards a new version of the PSL system that will allow for cell encapsulation in the prepolymer and that will result into cell-laden microfabricated 3D structures. This methodology will also be investigated to incorporate specific growth factors and complex spatial distribution of signaling molecule to dictate cell behavior and tissue response. These approaches will allow the seeding of multiple cell types in and on the scaffold and will move this technology towards functional tissue engineered cell-laden scaffolds.

5. Conclusion

This study demonstrates the capability of the PSL apparatus to engineer microscale 3D structures, supporting cell growth on precisely defined geometries. This fully automated bottom-up approach produced 3D constructs and enabled cell seeding, attachment and proliferation. The versatility of this technique used in combination with GelMA has resulted into both single layer (2D) and multilayer (3D) structures with precise internal architectures. It was shown that interconnectivity of pores allowed for uniform cell distribution throughout the scaffolds, resulting in high cell density and homogeneous distribution at the end of the culture period. Moreover, variation of the porous architecture and prepolymer concentration enabled tailoring the scaffolds mechanical properties. The combination of this microfabrication approach with photopolymerizable biomaterials will have implications in tissue engineering, for the study of structure-function relationship in tissues and the engineering of organs requiring precise spatial arrangement of cells and ECM within a 3D environment. By using this system it will be possible to produce biomimetic architectures based on microscale tissue properties and newly proposed structures relying on mathematical designs relying on the minimal surfaces theory. Moreover, localization of different biological and topographical cues, currently under investigation, will be used to study the influence of the scaffold properties on cell behavior and differentiation.

Supplementary Material

Refer to Web version on PubMed Central for supplementary material.

Acknowledgments

This work was supported by the National Institutes of Health (EB012597, HL092836, HL099073, and EB012597), the National Science Foundation (DMR0847287) and the Office of Naval Research. RG is the recipient of a postdoctoral fellowship from FQRNT.

References

1. Langer R, Vacanti JP. Tissue engineering. Science. 1993; 260(5110):920–926. [PubMed: 8493529]
2. Ingber DE, Mow VC, Butler D, Niklason L, Huard J, Mao J, et al. Tissue engineering and developmental biology: going biomimetic. Tissue Eng. 2006; 12(12):3265–3283. [PubMed: 17518669]
3. Hollister SJ. Porous scaffold design for tissue engineering. Nat Mater. 2005; 4(7):518–524. [PubMed: 16003400]
4. Cukierman E, Pankov R, Stevens DR, Yamada KM. Taking cell-matrix adhesions to the third dimension. Science. 2001; 294(5547):1708–1712. [PubMed: 11721053]
5. Supp DM, Boyce ST. Engineered skin substitutes: practices and potentials. Clin Dermatol. 2005; 23(4):403–412. [PubMed: 16023936]
6. Freed LE, Langer R, Martin I, Pellis NR, Vunjak-Novakovic G. Tissue engineering of cartilage in space. Proc Natl Acad Sci U S A. 1997; 94(25):13885–13890. [PubMed: 9391122]
7. Oberpenning F, Meng J, Yoo JJ, Atala A. De novo reconstitution of a functional mammalian urinary bladder by tissue engineering. Nat Biotechnol. 1999; 17(2):149–155. [PubMed: 10052350]
8. L'Heureux N, McAllister TN, de la Fuente LM. Tissue-engineered blood vessel for adult arterial revascularization. N Engl J Med. 2007; 357(14):1451–1453. [PubMed: 17914054]
9. Mikos AG, Herring SW, Ochareon P, Elisseeff J, Lu HH, Kandel R, et al. Engineering complex tissues. Tissue Eng. 2006; 12(12):3307–3339. [PubMed: 17518671]
10. Wake MC, Gupta PK, Mikos AG. Fabrication of pliable biodegradable polymer foams to engineer soft tissues. Cell Transplant. 1996; 5(4):465–473. [PubMed: 8800514]
11. Ma PX, Choi JW. Biodegradable polymer scaffolds with well-defined interconnected spherical pore network. Tissue Eng. 2001; 7(1):23–33. [PubMed: 11224921]
12. Harris LD, Kim BS, Mooney DJ. Open pore biodegradable matrices formed with gas foaming. J Biomed Mater Res. 1998; 42(3):396–402. [PubMed: 9788501]
13. Ellis DL, Yannas IV. Recent advances in tissue synthesis in vivo by use of collagen-glycosaminoglycan copolymers. Biomaterials. 1996; 17(3):291–299. [PubMed: 8745326]
14. Matthews JA, Wnek GE, Simpson DG, Bowlin GL. Electrospinning of collagen nanofibers. Biomacromolecules. 2002; 3(2):232–238. [PubMed: 11888306]
15. Zhou WY, Lee SH, Wang M, Cheung WL, Ip WY. Selective laser sintering of porous tissue engineering scaffolds from poly(L: -lactide)/carbonated hydroxyapatite nanocomposite microspheres. J Mater Sci Mater Med. 2008; 19(7):2535–2540. [PubMed: 17619975]
16. Holy CE, Fialkov JA, Davies JE, Shoichet MS. Use of a biomimetic strategy to engineer bone. J Biomed Mater Res A. 2003; 65(4):447–453. [PubMed: 12761834]
17. Engler AJ, Sen S, Sweeney HL, Discher DE. Matrix elasticity directs stem cell lineage specification. Cell. 2006; 126(4):677–689. [PubMed: 16923388]
18. Engelmayr GC Jr, Cheng M, Bettinger CJ, Borenstein JT, Langer R, Freed LE. Accordion-like honeycombs for tissue engineering of cardiac anisotropy. Nat Mater. 2008; 7(12):1003–1010. [PubMed: 18978786]
19. Park H, Larson BL, Guillemette MD, Jain SR, Hua C, Engelmayr GC Jr, et al. The significance of pore microarchitecture in a multi-layered elastomeric scaffold for contractile cardiac muscle constructs. Biomaterials. 2011; 32(7):1856–1864. [PubMed: 21144580]
20. Harley BA, Kim HD, Zaman MH, Yannas IV, Lauffenburger DA, Gibson LJ. Microarchitecture of three-dimensional scaffolds influences cell migration behavior via junction interactions. Biophys J. 2008; 95(8):4013–4024. [PubMed: 18621811]

21. Nichol JW, Koshy ST, Bae H, Hwang CM, Yamanlar S, Khademhosseini A. Cell-laden microengineered gelatin methacrylate hydrogels. Biomaterials. 2010; 31(21):5536–5544. [PubMed: 20417964]
22. Liu VA, Bhatia SN. Three-dimensional photopatterning of hydrogels containing living cells. Biomed Microdevices. 2002; 4(4):257–266.
23. Burdick JA, Khademhosseini A, Langer R. Fabrication of gradient hydrogels using a microfluidics/photopolymerization process. Langmuir. 2004; 20(13):5153–5156. [PubMed: 15986641]
24. Fukuda J, Khademhosseini A, Yeo Y, Yang X, Yeh J, Eng G, et al. Micromolding of photocrosslinkable chitosan hydrogel for spheroid microarray and co-cultures. Biomaterials. 2006; 27(30):5259–5267. [PubMed: 16814859]
25. Khademhosseini A, Langer R, Borenstein J, Vacanti JP. Microscale technologies for tissue engineering and biology. Proc Natl Acad Sci U S A. 2006; 103(8):2480–2487. [PubMed: 16477028]
26. Cuchiara MP, Allen AC, Chen TM, Miller JS, West JL. Multilayer microfluidic PEGDA hydrogels. Biomaterials. 2010; 31(21):5491–5497. [PubMed: 20447685]
27. Khademhosseini A, Langer R. Microengineered hydrogels for tissue engineering. Biomaterials. 2007; 28(34):5087–5092. [PubMed: 17707502]
28. West JL, Hubbell JA. Polymeric biomaterials with degradation sites for proteases involved in cell migration. Macromolecules. 1998; 32(1):241–244.
29. Benton JA, DeForest CA, Vivekanandan V, Anseth KS. Photocrosslinking of gelatin macromers to synthesize porous hydrogels that promote valvular interstitial cell function. Tissue Eng Part A. 2009; 15(11):3221–3230. [PubMed: 19374488]
30. Liu, Tsang V.; Chen, AA.; Cho, LM.; Jadin, KD.; Sah, RL.; DeLong, S., et al. Fabrication of 3D hepatic tissues by additive photopatterning of cellular hydrogels. FASEB J. 2007; 21(3):790–801. [PubMed: 17197384]
31. Lu Y, Mapili G, Suhali G, Chen S, Roy K. A digital micro-mirror device-based system for the microfabrication of complex, spatially patterned tissue engineering scaffolds. J Biomed Mater Res A. 2006; 77(2):396–405. [PubMed: 16444679]
32. Dhariwala B, Hunt E, Boland T. Rapid prototyping of tissue-engineering constructs, using photopolymerizable hydrogels and stereolithography. Tissue Eng. 2004; 10(9e10):1316–1322. [PubMed: 15588392]
33. Seitz H, Rieder W, Irsen S, Leukers B, Tille C. Three-dimensional printing of porous ceramic scaffolds for bone tissue engineering. J Biomed Mater Res Part B. 2005; 74(2):782–788.
34. Chan V, Zorlutuna P, Jeong JH, Kong H, Bashir R. Three-dimensional photo-patterning of hydrogels using stereolithography for long-term cell encapsulation. Lab Chip. 2010; 10(16):2062–2070. [PubMed: 20603661]
35. Lee JW, Lan PX, Kim B, Lim G, Cho D-W. 3D scaffold fabrication with PPF/DEF using micro-stereolithography. Microelec Eng. 2010; 84(5–8):1702–1705.
36. Melchels FP, Bertoldi K, Gabbrielli R, Velders AH, Feijen J, Grijpma DW. Mathematically defined tissue engineering scaffold architectures prepared by stereolithography. Biomaterials. 2010; 31(27):6909–6916. [PubMed: 20579724]
37. Melchels FP, Feijen J, Grijpma DW. A review on stereolithography and its applications in biomedical engineering. Biomaterials. 2010; 31(24):6121–6130. [PubMed: 20478613]
38. Hsieh TM, Ng CW, Narayanan K, Wan AC, Ying JY. Three-dimensional micro-structured tissue scaffolds fabricated by two-photon laser scanning photolithography. Biomaterials. 2010; 31(30): 7648–7652. [PubMed: 20667410]
39. Melchels FP, Barradas AM, van Blitterswijk CA, de Boer J, Feijen J, Grijpma DW. Effects of the architecture of tissue engineering scaffolds on cell seeding and culturing. Acta Biomaterialia. 2010; 6(11):4208–4217. [PubMed: 20561602]
40. Han LH, Suri S, Schmidt CE, Chen S. Fabrication of three-dimensional scaffolds for heterogeneous tissue engineering. Biomed Microdevices. 2010; 12(4):721–725. [PubMed: 20393801]
41. Han L-H, Mapili G, Chen S, Roy K. Projection microfabrication of three-dimensional scaffolds for tissue engineering. J Manuf Sci Eng. 2008; 130(2):1005–1009.

42. Choi J-W, Wicker R, Lee S-H, Choi K-H, Ha C-S, Chung I. Fabrication of 3D biocompatible/biodegradable micro-scaffolds using dynamic mask projection microstereolithography. J Mater Process Technol. 2009; 209(15–16):5494–5503.
43. Van Den Bulcke AI, Bogdanov B, De Rooze N, Schacht EH, Cornelissen M, Berghmans H. Structural and rheological properties of methacrylamide modified gelatin hydrogels. Biomacromolecules. 2000; 1(1):31–38. [PubMed: 11709840]
44. Rajagopalan S, Robb RA. Schwarz meets Schwann: design and fabrication of biomorphic and durataxic tissue engineering scaffolds. Med Image Anal. 2006; 10(5):693–712. [PubMed: 16890007]
45. Yoo DJ. Computer-aided porous scaffold design for tissue engineering using triply periodic minimal surfaces. Int J Precis Eng Man. 2011; 12(1):61–67.
46. Yoo DJ. Porous scaffold design using the distance field and triply periodic minimal surface models. Biomaterials. 2011; 32(31):7741–7754. [PubMed: 21798592]
47. Costa HS, Pereira MM, Andrade GI, Stancioli EB, Mansur HS. Characterization of calcium phosphate coating and zinc incorporation on porous alumina scaffolds. Mat Res. 2007; 10:27–29.
48. Ou-Yang H, Paschalis EP, Mayo WE, Boskey AL, Mendelsohn R. Infrared microscopic imaging of bone: spatial distribution of CO3(2-). J Bone Miner Res. 2001; 16(5):893–900. [PubMed: 11341334]
49. Aubin H, Nichol JW, Hutson CB, Bae H, Sieminski AL, Cropek DM, et al. Directed 3D cell alignment and elongation in microengineered hydrogels. Biomaterials. 2011; 31(27):6941–6951. [PubMed: 20638973]
50. Luo Y, Shoichet MS. A photolabile hydrogel for guided three-dimensional cell growth and migration. Nat Mater. 2004; 3(4):249–253. [PubMed: 15034559]
51. West JL, Hubbell JA. Comparison of covalently and physically cross-linked polyethylene glycol-based hydrogels for the prevention of postoperative adhesions in a rat model. Biomaterials. 1995; 16(15):1153–1156. [PubMed: 8562791]
52. DeLong SA, Moon JJ, West JL. Covalently immobilized gradients of bFGF on hydrogel scaffolds for directed cell migration. Biomaterials. 2005; 26(16):3227–3234. [PubMed: 15603817]
53. Fozdar DY, Soman P, Lee JW, Han LH, Chen S. Three-dimensional polymer constructs exhibiting a tunable negative Poisson's ratio. Adv Funct Mater. 2011; 21(14):2712–2720. [PubMed: 21841943]
54. Saha K, Pollock JF, Schaffer DV, Healy KE. Designing synthetic materials to control stem cell phenotype. Curr Opin Chem Biol. 2007; 11(4):381–387. [PubMed: 17669680]
55. Lutolf MP, Hubbell JA. Synthetic biomaterials as instructive extracellular microenvironments for morphogenesis in tissue engineering. Nat Biotechnol. 2005; 23(1):47–55. [PubMed: 15637621]
56. Zeltinger J, Sherwood JK, Graham DA, Mueller R, Griffith LG. Effect of pore size and void fraction on cellular adhesion, proliferation, and matrix deposition. Tissue Eng. 2001; 7(5):557–572. [PubMed: 11694190]
57. Freed LE, Guilak F, Guo XE, Gray ML, Tranquillo R, Holmes JW, et al. Advanced tools for tissue engineering: scaffolds, bioreactors, and signaling. Tissue Eng. 2006; 12(12):3285–3305. [PubMed: 17518670]
58. Grayson WL, Martens TP, Eng GM, Radisic M, Vunjak-Novakovic G. Biomimetic approach to tissue engineering. Semin Cell Dev Biol. 2009; 20(6):665–673. [PubMed: 19146967]
59. Borenstein JT, Weinberg EJ, Orrick BK, Sundback C, Kaazempur-Mofrad MR, Vacanti JP. Microfabrication of three-dimensional engineered scaffolds. Tissue Eng. 2007; 13(8):1837–1844. [PubMed: 17590149]
60. Mann BK, West JL. Cell adhesion peptides alter smooth muscle cell adhesion, proliferation, migration, and matrix protein synthesis on modified surfaces and in polymer scaffolds. J Biomed Mater Res. 2002; 60(1):86–93. [PubMed: 11835163]
61. Gobin AS, West JL. Val-ala-pro-gly, an elastin-derived non-integrin ligand: smooth muscle cell adhesion and specificity. J Biomed Mater Res A. 2003; 67(1):255–259. [PubMed: 14517884]
62. Burdick JA, Anseth KS. Photoencapsulation of osteoblasts in injectable RGD-modified PEG hydrogels for bone tissue engineering. Biomaterials. 2002; 23(22):4315–4323. [PubMed: 12219821]

63. Rowe SL, Stegemann JP. Interpenetrating collagen-fibrin composite matrices with varying protein contents and ratios. Biomacromolecules. 2006; 7(11):2942–2948. [PubMed: 17096517]

64. Moutos FT, Freed LE, Guilak F. A biomimetic three-dimensional woven composite scaffold for functional tissue engineering of cartilage. Nat Mater. 2007; 6(2):162–167. [PubMed: 17237789]

65. Discher DE, Janmey P, Wang YL. Tissue cells feel and respond to the stiffness of their substrate. Science. 2005; 310(5751):1139–1143. [PubMed: 16293750]

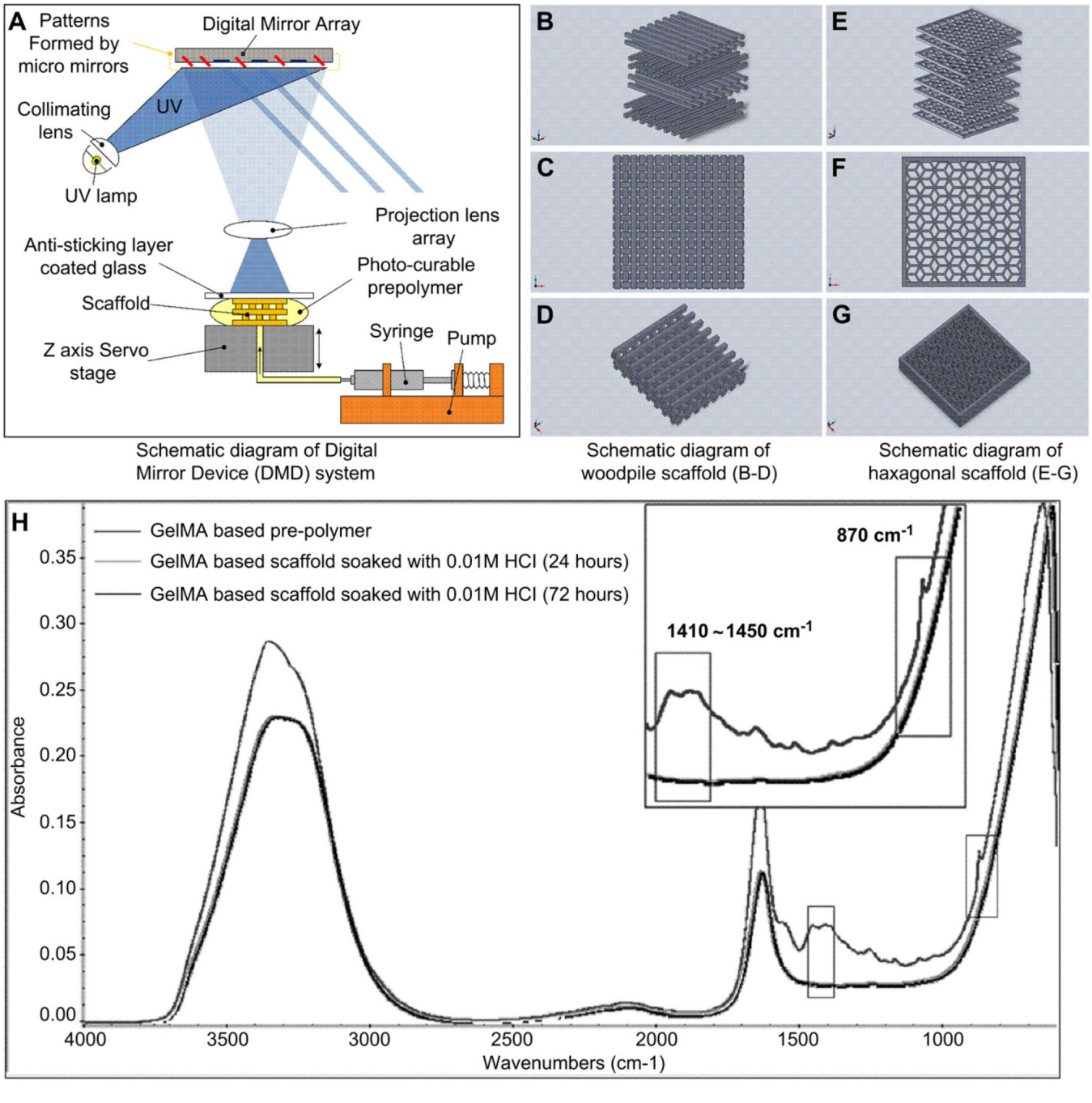

Schematic diagram of Digital Mirror Device (DMD) system

Schematic diagram of woodpile scaffold (B-D)

Schematic diagram of haxagonal scaffold (E-G)

Fig. 1.

Schematic representation of the PSL apparatus (A) and the engineered structures generated using a CAD software used for scaffold design and fabrication (B–G). The layers of crosslinked GelMA can be stacked to form scaffolds having log pile (B–D) or hexagonal (E–G) structures. The chemical properties of the material were measured by FTIR prior to photocrosslinking and following incubation in 0.01 M HCl (H). FTIR spectra shows prepolymer (upper curve) and scaffold properties after incubation in HCl (lower curves). The peaks observed for the prepolymer solution at 1410–1450 cm^{-1} and 870 cm^{-1}, attributed to the presence of CO_3^{-2} in the material, were not found in the scaffolding material

(magnified sections of the curve). These results demonstrate complete removal of $CaCO_3$ microparticles from the scaffolds by incubation in HCL prior to the cell seeding process.

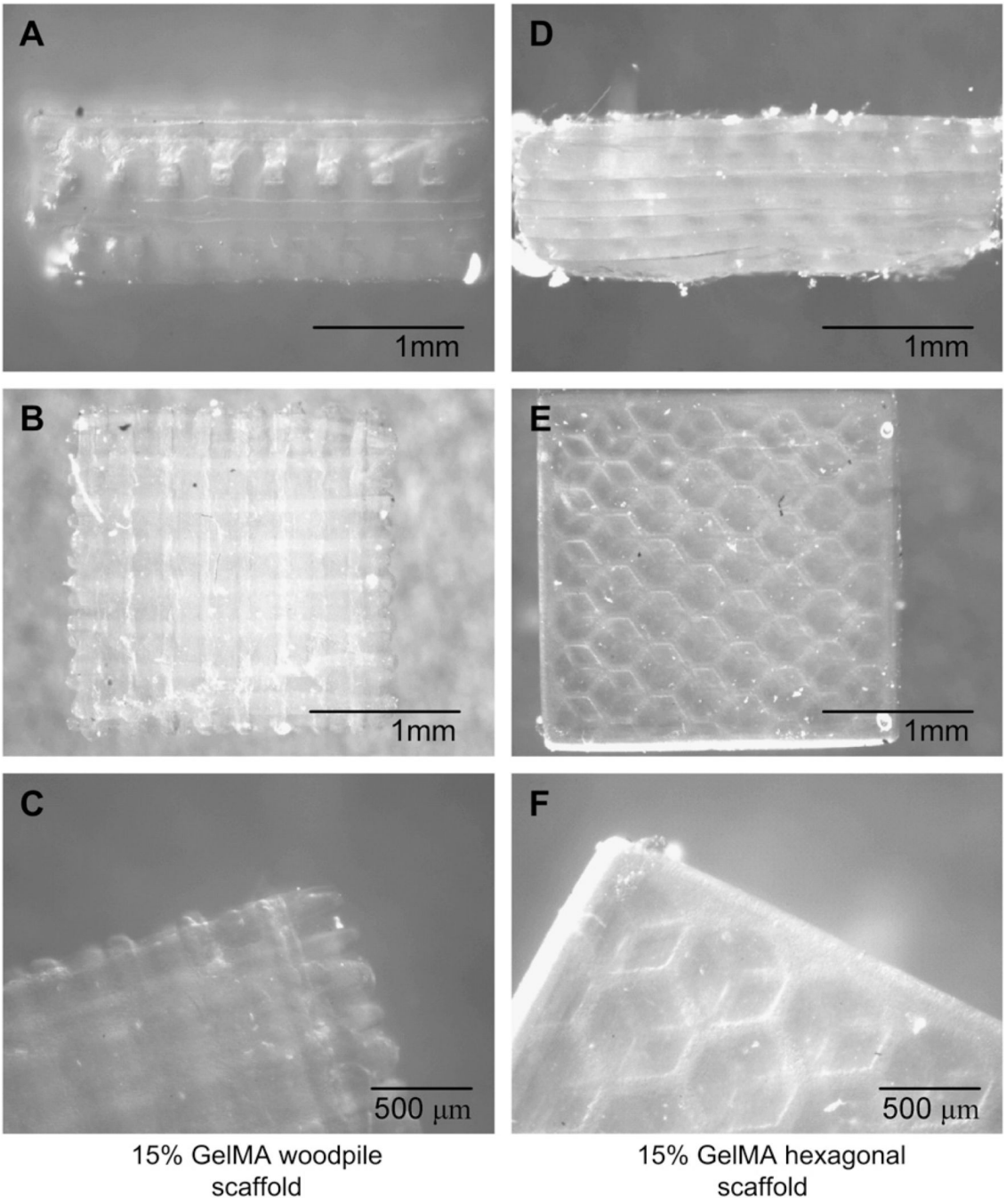

Fig. 2.

Woodpile (A–C) and hexagonal structures (D–F) produced using the PSL system according to the engineered CAD files, using a 15% GelMA prepolymer solution. The PSL fabrication process produced precise features using a system of dynamic masks generated by a digital light controlling chip. Figures A, B and D, E show side and top views of the woodpile and hexagonal scaffolds respectively. Figures C and F show a magnification of the assembled structures.

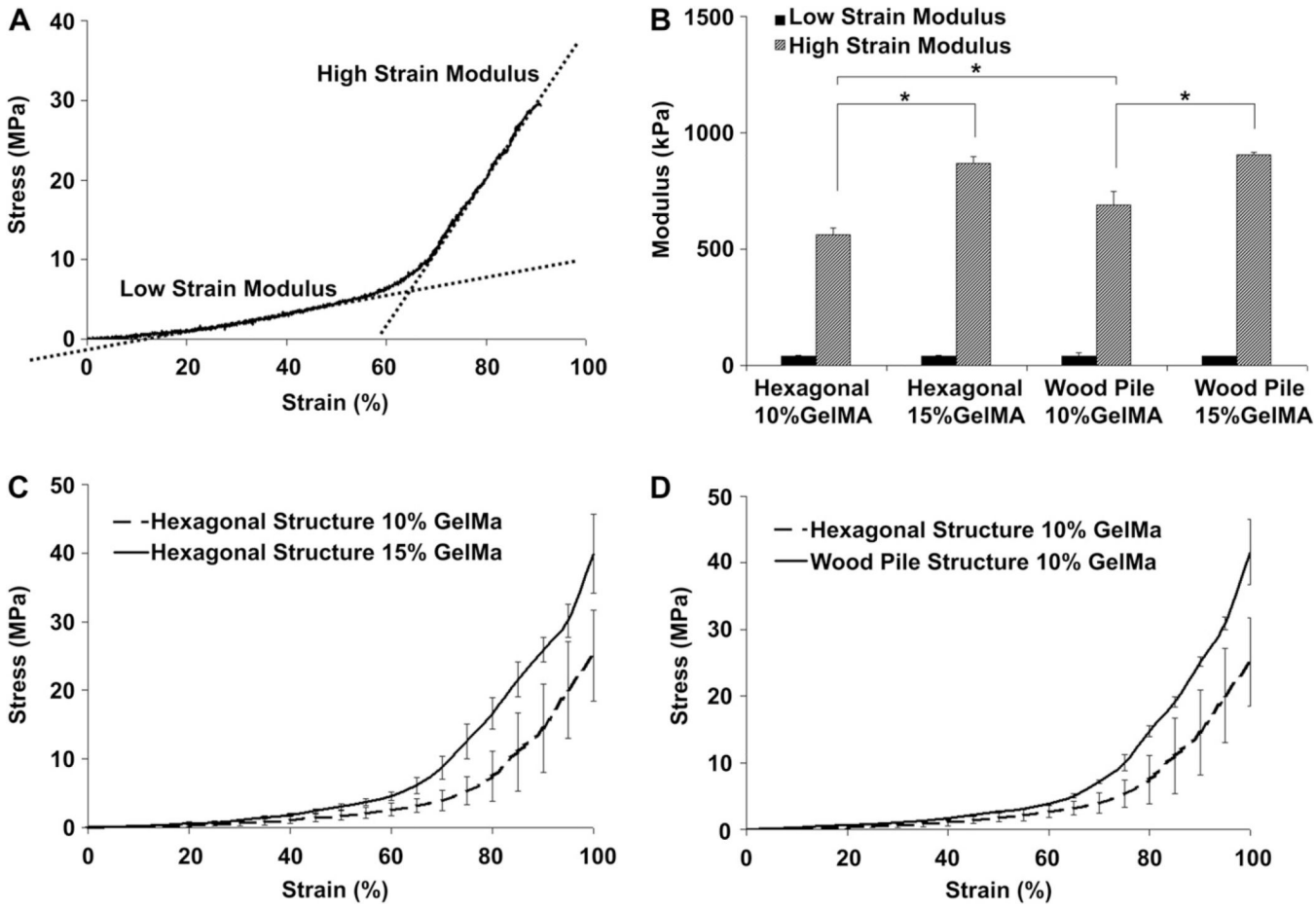

Fig. 3.

Mechanical properties of PSL-fabricated scaffolds having hexagonal or log pile structures and fabricated using various GelMA percentages. A characteristic stress-strain curve displaying low-strain and high-strain compressive moduli was obtained for every sample tested (A). Results showed that high-strain modulus was significantly increased for both hexagonal and woodpile structures when the percentage of GelMA was increased form 10%–15%, whereas no significant difference was seen for the low-strain modulus in any conditions (B). Compressive testing results indicate that prepolymer concentration (C) and engineered structures (D) can be used to tailor the mechanical properties of the GelMA scaffolds. * indicates statistical significance ($p < 0.05$).

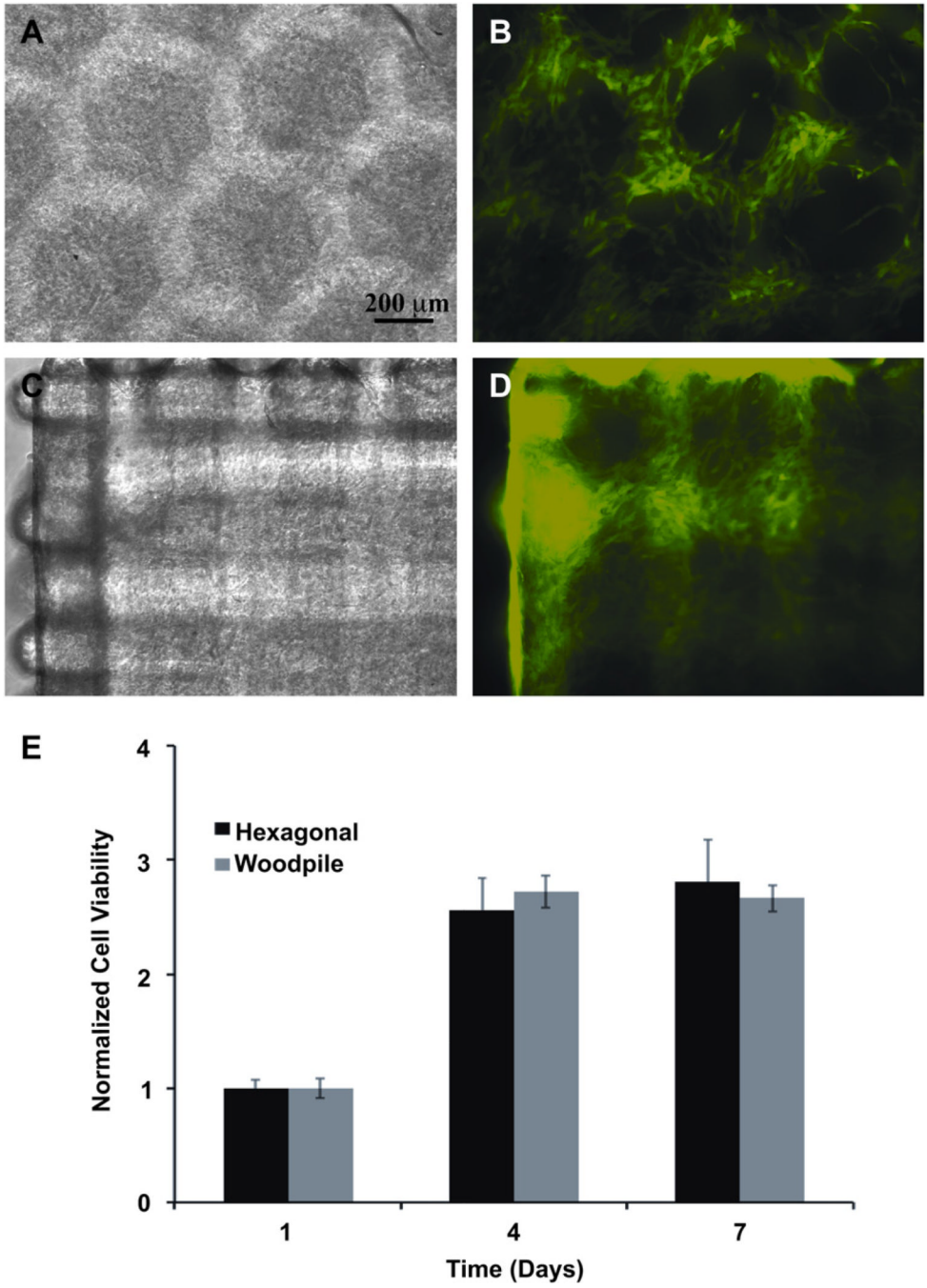

Fig. 4.

Hexagonal (A, B) and woodpile (C, D) scaffolds were seeded with HUVEC-GFP (B, D) to demonstrate the ability of the engineered structures to support cell adhesion and growth. Cell viability was assessed using a MTS assay (E). Results showed an increase in the number of cells throughout the culture period, indicating the adequate compatibility of the scaffolding material with the cells.

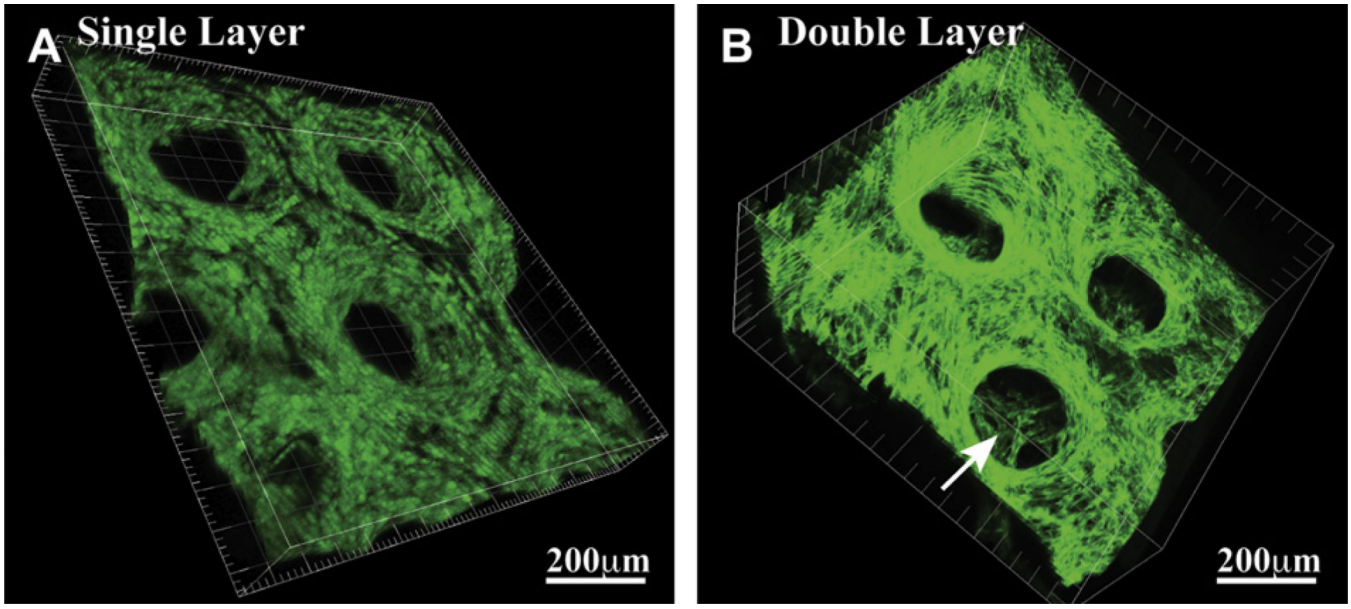

Fig. 5.

3D confocal imaging of the HUVEC-GFP seeded scaffolds showing the capability of the PSL system to generate (A) single and (B) multiple layers assembly having precisely defined geometries. These images, taken 4 days following cell seeding, also demonstrate the efficiency of the seeding method and the structural stability of the scaffold, as the features initially engineered in the 3D structure remain present throughout the culture period.

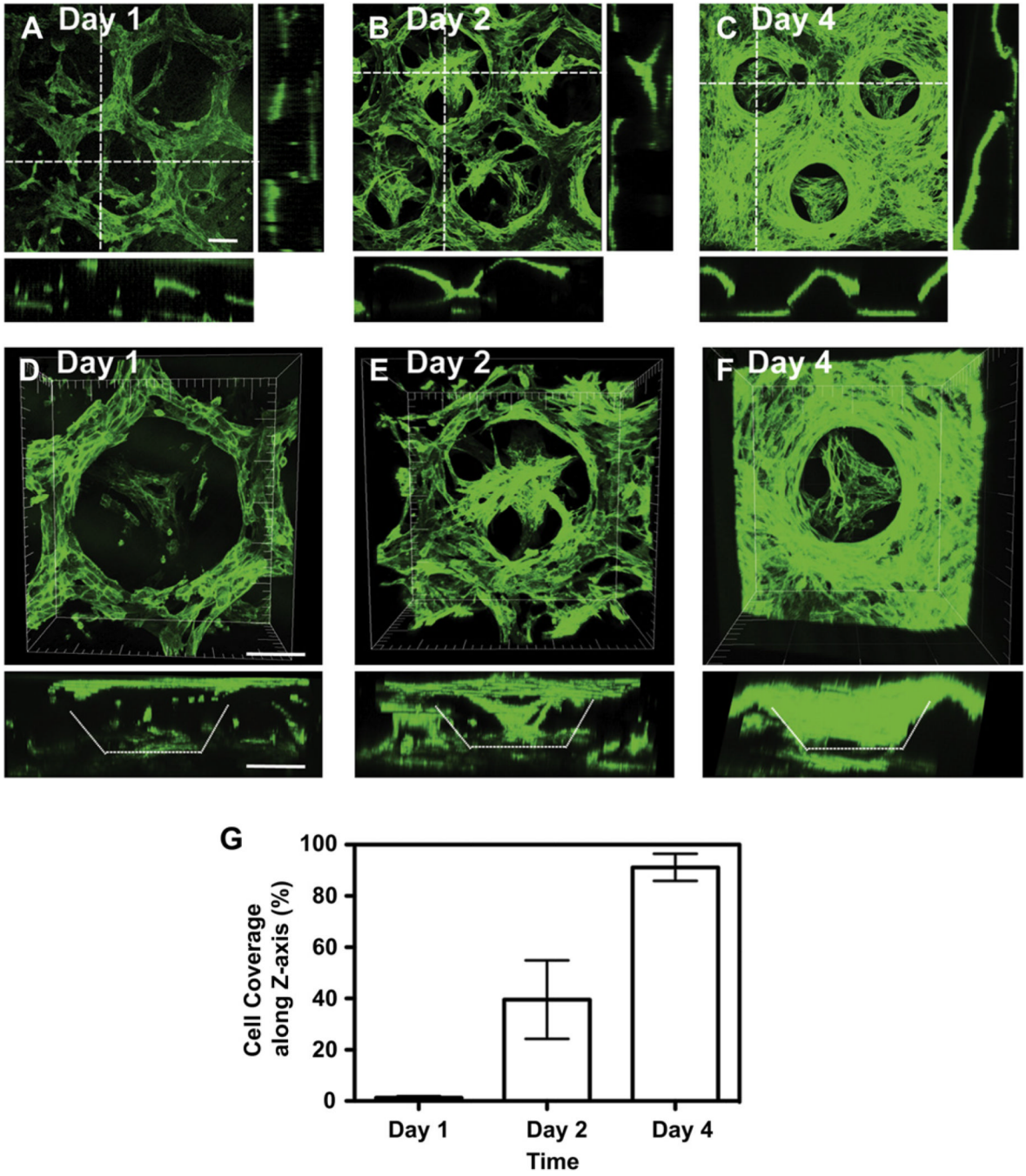

Fig. 6.

3D confocal images showing scaffold coverage by the HUVEC-GFP cells (A, B, C) and cell penetration into the porous structure (D, E, F) as a function of time. Images taken at day 1 (A, D), 2 (B,E) and 4 (C, F) showed an increase in cell number and penetration depth, as well as an enhanced scaffold coverage by the cells resulting into a confluent layer on the 3D strucure at day 4 (91+/−5%) (G). Scale bar = 100 μm.

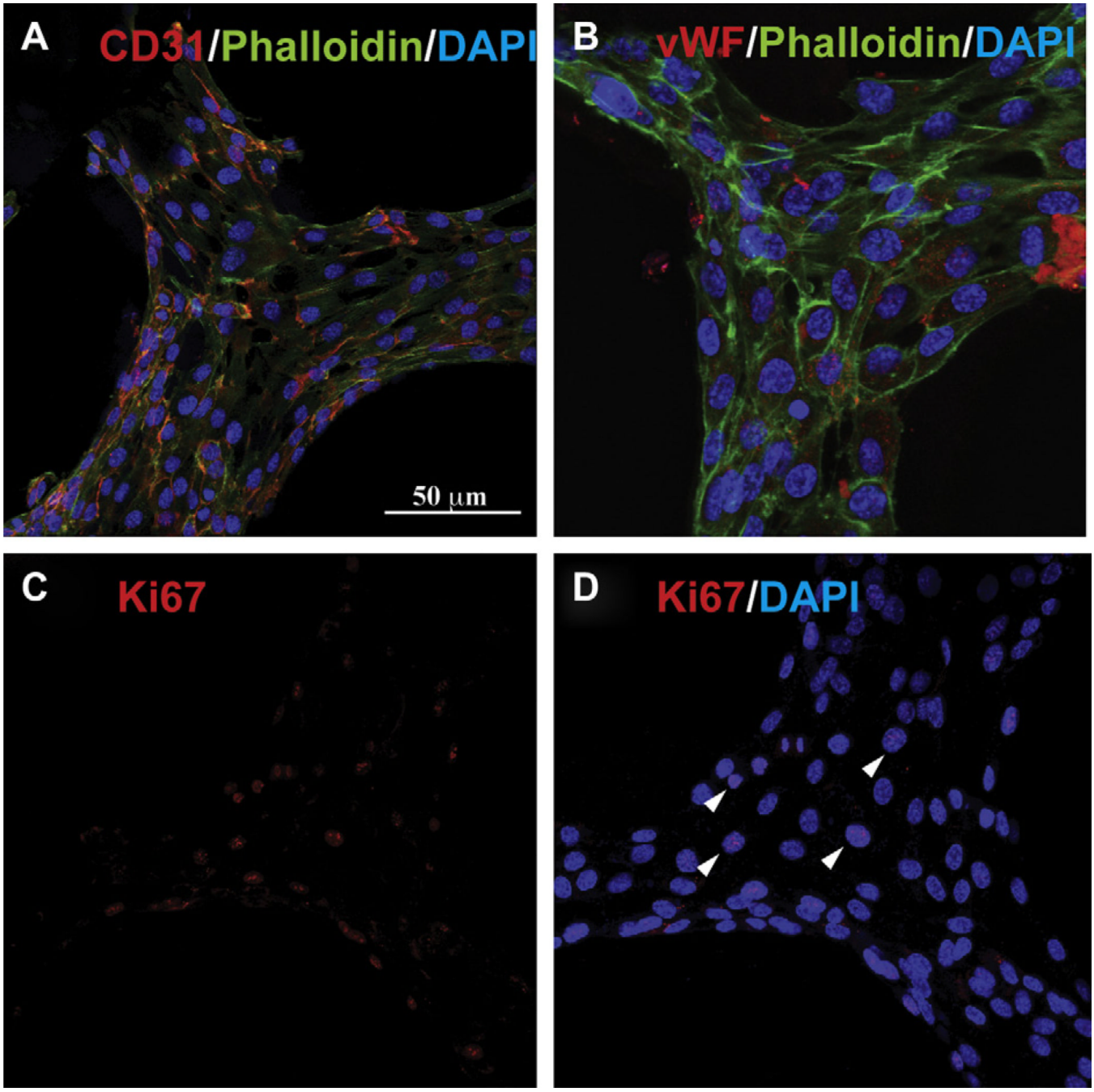

Fig. 7.

Immunofluorescence images showing the biological functionality of the HUVEC seeded scaffolds. The presence of endothelial cell specific markers CD31 (A) and vonWillebrand factor (vWF; B) showed that the confluent endothelial cells retained their phenotype during the culture period. Moreover, Ki67 labeling (C) showed HUVEC adhered on the scaffolds and expressing this marker (arrows, D), indicating a proliferative state after 4 days in culture.